



Article

Fractal Features of Muscle to Quantify Fatty Infiltration in Aging and Pathology

Annamaria Zaia ^{1,*} , Martina Zannotti ² , Lucia Losa ² and Pierluigi Maponi ²

¹ Center of Innovative Models for Ageing Care and Technology, Scientific Direction, IRCCS INRCA, 60121 Ancona, Italy

² School of Science and Technology, University of Camerino (MC), 62032 Camerino, Italy; martina.zannotti@studenti.unicam.it (M.Z.); lucia.loso@studenti.unicam.it (L.L.); pierluigi.maponi@unicam.it (P.M.)

* Correspondence: a.zaia@inrca.it

Abstract: The physiological loss of muscle mass and strength with aging is referred to as “sarcopenia”, whose combined effect with osteoporosis is a serious threat to the elderly, accounting for decreased mobility and increased risk of falls with consequent fractures. In previous studies, we observed a high degree of inter-individual variability in paraspinal muscle fatty infiltration, one of the most relevant indices of muscle wasting. This aspect led us to develop a computerized method to quantitatively characterize muscle fatty infiltration in aging and diseases. Magnetic resonance images of paraspinal muscles from 58 women of different ages (age range of 23–85 years) and physio-pathological status (healthy young, pre-menopause, menopause, and osteoporosis) were used to set up a method based on fractal-derived texture analysis of lean muscle area (contractile muscle) to estimate muscle fatty infiltration. In particular, lacunarity was computed by parameter β from the GBA (gliding box algorithm) curvilinear plot fitted by our hyperbola model function. Succolarity was estimated by parameter μ , for the four main directions through an algorithm implemented with this purpose. The results show that lacunarity, by quantifying muscle fatty infiltration, can discriminate between osteoporosis and healthy aging, while succolarity can separate the other three groups showing similar lacunarity. Therefore, fractal-derived features of contractile muscle, by measuring fatty infiltration, can represent good indices of sarcopenia in aging and disease.



Citation: Zaia, A.; Zannotti, M.; Losa, L.; Maponi, P. Fractal Features of Muscle to Quantify Fatty Infiltration in Aging and Pathology. *Fractal Fract.* **2024**, *8*, 275. <https://doi.org/10.3390/fractalfract8050275>

Academic Editor: Didier Delignières

Received: 22 February 2024

Revised: 22 April 2024

Accepted: 24 April 2024

Published: 6 May 2024



Copyright: © 2024 by the authors. Licensee MDPI, Basel, Switzerland. This article is an open access article distributed under the terms and conditions of the Creative Commons Attribution (CC BY) license (<https://creativecommons.org/licenses/by/4.0/>).

Keywords: aging; biocomplexity; biomarkers; fractal; fatty infiltration; lacunarity; magnetic resonance imaging; muscle; sarcopenia; succolarity

1. Introduction

Aging is characterized by a progressive structural and functional decline at different levels. Such a decline also affects the musculoskeletal apparatus. Quantitative and qualitative changes occurring at skeletal muscles with aging account for increased prevalence of disability, and increased risk of morbidity and mortality in old adults [1–4]. The combined effect of sarcopenia and osteoporosis (osteosarcopenia, another main age-related disease) is a devastating threat to the old adults, leading to reduced mobility and increased risk for falls and subsequent fractures. The prevalence of osteosarcopenia varies in a range of 5–38% in old people depending on the study design and on the classification of sarcopenia [5]. Sarcopenia is a generalized phenomenon affecting all skeletal muscles. It has been associated with osteoporosis in women following a hip fragility fracture, while the prevalence of sarcopenia in patients with vertebral fragility fractures is poorly investigated [6,7]. In previous studies on osteoporosis and vertebral fracture risk, we observed a high degree of inter-individual variability in paraspinal muscle fatty infiltration. This aspect led us to develop a computerized method to quantitatively characterize muscle fatty infiltration of paraspinal muscle in aging and osteoporosis. The term sarcopenia was introduced by Rosenberg in 1989 [8,9] to define the physiological loss of muscle mass with aging. More

recently, sarcopenia has been defined as “a syndrome characterized by a progressive and generalized loss of skeletal muscle mass and strength with a risk of adverse outcomes such as physical disability, poor quality of life and death” [10,11]. Past the age of 50 years, the rate of muscle loss ranges within 1–2% a year. It accounts for 25% and 40% sarcopenic people after the age of 70 and 80 years, respectively [12,13]. The term myopenia has been proposed to define a clinically relevant degree of muscle wasting characterized by a rapid loss of muscle mass in a short time (i.e., more than 5% in 6–12 months) associated with harmed functional capacity and increased risk of morbidity and mortality [14].

Several aspects other than muscle size lead to the loss of physical activity strength in the etiology of disability. Both neurological and muscular factors lead to the decline of muscle strength [15–18]: muscle atrophy, reduced contractile quality induced by impaired myofibrillar machinery, and fatty infiltration of contractile muscle [3,4,15,19].

Among several techniques proposed for muscle assessment [20], three main medical imaging systems are normally employed in the evaluation of muscle mass variation with aging: computer tomography (CT), magnetic resonance imaging (MRI), and dual-energy X-ray absorptiometry (DXA). Although CT and MRI represent the gold standards for muscle mass estimate, their application has been limited to the research field, while DXA has been chosen for clinical use [21,22]. In fact, DXA, in spite of supplying surrogate estimates of both regional and whole-body skeletal muscle mass, is widely diffused as it is cheap and enables limited radiation exposure. Ultrasonography (US) is another imaging technique widely used for qualitative and quantitative assessment of muscle. US is a portable, non-ionizing and non-invasive cheap technique for muscle properties’ estimation showing positive correlation with muscle measurements obtained by the other imaging techniques. Nevertheless, US presents the limitations of poor reproducibility and accuracy [23]. Both CT and MRI represent imaging techniques very precise in differentiating fat from other soft tissues; however, MRI has been recognized as the best tool for fatty infiltration assessment [24]. Numerous and different techniques have been proposed to assess muscle fatty infiltration; nevertheless, there is a lack of methods for its quantitative estimate [25–29].

The aim of this study was to set up a computerized method for quantitative characterization of fatty infiltration of the contractile muscle. Considering that the term ‘fatty infiltration’ has been using with a non-univocal meaning [30], it has to be stressed that the term ‘fatty infiltration’ in this study identifies inter- and intra-non-contractile tissue (mainly fat and connective tissue) that substitutes myofibrillar tissue portions within the lean muscle area (contractile muscle).

Image texture analysis is a key approach to understand the relationships between the microstructures of the tissues under consideration and their properties. Different approaches can be used to extract image texture features [31] and the statistical approach based on the co-occurrence matrix [32] is probably the most common approach. Paradigms such as complexity, chaos, and fractality, introduced in the field of biomedicine and gerontology in particular, are sources of new approaches and tools to their study. The proposed method, set up considering the complexity of living beings and the fractality of many structures and functions of humans, can be seen as a model-based approach; in fact, it aims to estimate the fractal features of LeanCSA (lean muscle cross-sectional area) in MR images of paraspinal muscles. In particular, the hyperbola-based method was used for lacunarity texture analysis; it provides three parameters (α , β , γ), for which α correlates with the fractal dimension and β quantifies the lacunarity of the set, while γ represents the translation term on x axis [33–36]. Mandelbrot introduced the term ‘lacunarity’ (from the Latin *lacuna*, which means ‘gap or hole’) to characterize fractal objects with the same fractal dimension but differently appearing [37]. Later, lacunarity analysis was also introduced as a more general texture analysis method to describe complex patterns with or without fractal properties [38]. Succolarity, the other fractal-derived feature, was also considered to complete the characterization of muscle fatty infiltration. Succolarity (from the Latin *succolare* < *sub* + *colare*, which means ‘to filter, strain, purify’ and is associated with *percolare*, which means ‘to strain or filter through, to percolate’) was introduced by Mandelbrot [39] to discriminate fractals with the same lacunarity. Succolarity quantifies the

capacity of a hypothetical fluid to percolate in a given direction such that it can estimate the connectivity and the intercommunication in the structure of a set [40]. Parameter μ for the four main directions was introduced to quantify succolarity by using a revised version of the method proposed to compute succolarity [41]. While fractal dimension and lacunarity are widely used, succolarity was not considered for a long time after its introduction in fractal geometry. More recently, the concept of succolarity has been revisited and quantification has been also proposed [42]. In the following, with the misuse of the terminology, we refer to such parameters as fractal features for the sake of brevity as they were born to better characterize fractal objects even if, later, they were also introduced as more general texture analyses to characterize complex objects with or without fractal properties.

In this study, fractal-derived texture analysis was applied to lumbar paraspinal muscle MRI axial images acquired by the multislice spin-echo technique from subjects of different age and physio-pathological status to verify the potential of fractal parameters as new indices of muscle wasting in aging (sarcopenia) and age-related pathology (osteoporosis). Classic indices of muscle mass composition were also considered, together with a new one, namely the Lean/Fat ratio. This new index, derived from classic measurements, relates changes occurring at both lean and fatty muscle mass, thus allowing for a better comparison between classic and fractal-based new methods.

2. Materials and Methods

2.1. Description of Dataset

2.1.1. Subjects

The data used in this study were from subjects enrolled in a previous study on vertebral trabecular bone degeneration in aging and osteoporosis [33,34]. In particular, the dataset considered in this study included women within the age range of 23–81 years stratified in groups on the basis of their physio-pathological status (healthy young, pre-menopause, menopause, osteoporosis). Table 1 summarizes the main demographic and clinical characteristics of the subjects under study. MRI images of lumbar spine were used to quantify paraspinal muscle degeneration with aging and pathology.

Table 1. Demographic and clinical characteristics of subjects' sample.

Subjects	Number	Age Range	Mean Age ¹	Median Age
All	59	23–81	53 ± 15	50
Young	15	23–40	35 ± 5	37
Pre-menopause	15	42–50	45 ± 3	44
Menopause	14	51–81	64 ± 10	64
Osteoporosis ²	15	57–78	70 ± 6	71
Age-matched ³	10	56–81	68 ± 8	67

¹ Mean age expressed as mean ± SD (standard deviation); ² T-score ≤ −2.5 as defined by the World Health Organization; ³ age-matched control group for comparison with osteoporosis group.

This study was carried out according to the Declaration of Helsinki. All subjects included in this study gave their consent to use MRI scan data for research scope.

2.1.2. MRI Image Acquisition

High-resolution MRI, 1.5T whole-body system (Gyrosan Intera; Philips-Medical System, Milano, Italy, ACR-Nema 1.0), was used for lumbar spine scans using a phased array dS Spine coil. The spin-echo multislice technique was applied to acquire axial section images of L1–L4 lumbar spine (9 slices/vertebra with a thickness of 3 mm without a space gap between slices). The pulse sequence used was TE of 15 ms, TR of 525 ms; the flip angle was of 90°, matrix 512 × 512 pixel, and the pixel size equal to 0.469 mm. The scan time was shorter than 15 min.

2.2. Image Processing and Analysis

MR images of the 4th lumbar vertebra were used to characterize paraspinal muscles. The MRI dataset was transferred to a personal computer for image texture analysis.

2.2.1. Analysis of MR Images

The algorithms developed for the characterization of lumbar paraspinal muscles start with an image area selection by a semi-automatic procedure to define the region of interest (ROI) corresponding to the lumbar paraspinal muscle group considered. This ROI was used to delimit lean muscle area (contractile area) and the surrounding fatty muscle area. A simple count of pixel numbers belonging to these ROIs was performed for muscle composition estimation by classic indices such as cross-sectional area of the whole muscle mass (TotCSA), lean muscle mass (LeanCSA) and fatty muscle mass (FatCSA). The percentage of lean and fatty mass, and the ratio between lean and fatty mass (Lean/Fat ratio) were also calculated.

LeanCSA was considered to quantify fatty infiltration by three independent indices:

- ρ : the ratio between lean (contractile) and fatty (non-contractile) portions of muscle tissue belonging to the lean muscle area (LeanCSA);
- β : the lacunarity of lean muscle area, where fatty infiltration is assumed as lacunae;
- μ : the succolarity of LeanCSA, where fatty infiltration is assumed as the empty space within the muscle tissue which is percolated by a hypothetical fluid crossing the set in four directions (down to up \uparrow ; left to right \rightarrow ; up to down \downarrow ; right to left \leftarrow).

The computational procedures to obtain these indices from LeanCSA are described below. These indices were compared with the classic indices of muscle composition described above. Figure 1 shows details of paraspinal muscle MRI from subjects of different age where the age-related increase in fatty infiltration is well observable. Figure 2 (left) shows a sketch of ROIs' selection for both muscle composition and fatty infiltration estimates.

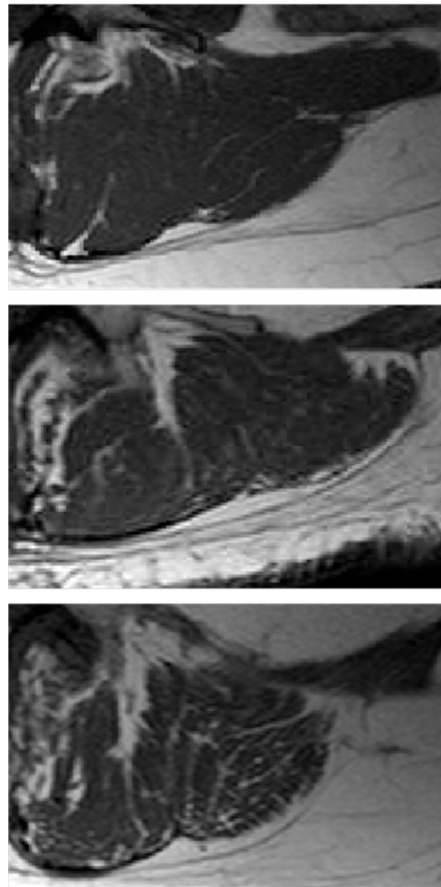


Figure 1. Paraspinal muscle fatty infiltration. Examples of paraspinal muscle MRI from subjects of different age and physio-pathological status: **(top)** young, 31 years; **(middle)** old, 71 years; **(bottom)** osteoporotic, 71 years. The age-related increasing branching of fatty infiltration with a fractal tree like pattern is more evident in osteoporosis than in 'healthy' aging.

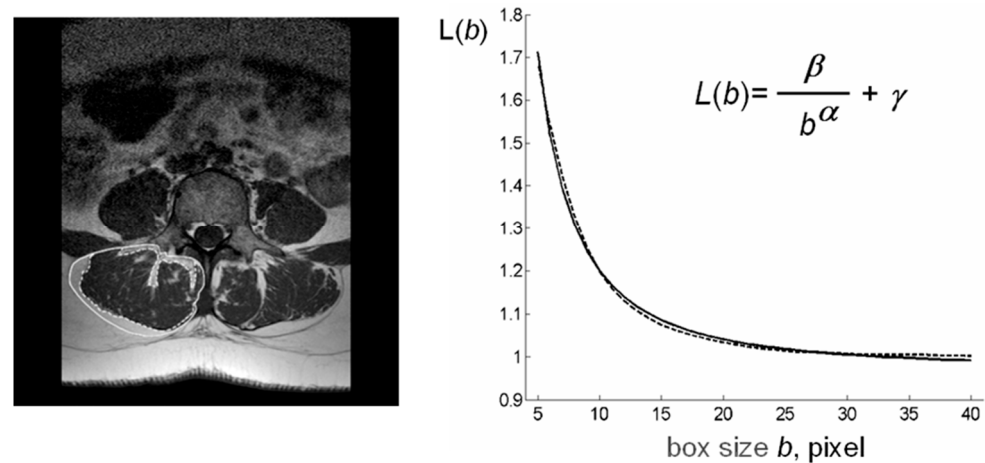


Figure 2. Schematic representation of lacunarity method. (left) Paraspinal muscle MRI-spin-echo to visualize muscle CSA at level of the 4th lumbar vertebra with ROIs selection to delimit TotCSA (solid line) and separate LeanCSA and FatCSA (dotted line); (right) GBA curvilinear plot (dotted line) as fitted by our hyperbola model function $L(b)$ (solid line) to compute the triplet of parameters α^* , β^* , γ^* ; parameter α correlates with fractal dimension and parameter β describes the concavity of the curve and gives a quantitative estimate of lacunarity. MRI: magnetic resonance imaging, CSA: cross-sectional area, GBA: gliding box algorithm.

2.2.2. Computation of Index ρ (Lean/Fat Ratio)

The algorithm to compute ρ is based on a simple count of pixels n_L (contractile muscle) and the pixels n_F (non-contractile muscle) belonging to the lean mass area (LeanCSA). The ratio between these two numbers gives the value of the index ρ , which is as follows:

$$\rho = \frac{n_L}{n_F} \quad (1)$$

At a first glance, the decision of whether a given pixel belongs to the lean mass or to the fatty mass seems to be quite simple; in fact, fatty mass is characterized by a lighter gray level than the lean mass. However, the non-uniform illumination in the image can make it difficult to obtain a unique threshold to separate the lean mass from the fatty mass. Therefore, a simple adaptive thresholding procedure is used. The bounding box of the ROI is uniformly partitioned in M by N rectangles and a different threshold is computed for the rectangles with a not empty intersection with the ROI. Let R be the intersection of the ROI and one of such rectangles, and H the histogram of gray levels in R ; so, $H(i)$ gives the number of pixels in R with a gray level i , where $i = 0, 1, \dots, 255$. The following Algorithm 1 is used to compute the threshold τ in R .

Algorithm 1: (local threshold). Given the sub-image R , the histogram H of gray levels in R , and a tolerance T , compute the threshold τ by the following steps

- let τ_1 be the index of the relative maximum of H that is closest to $i = 0$;
- let τ_2 be the index of the relative maximum of H that is closest to $i = 255$;
- let $\tau = (\tau_1 + \tau_2)/2$;
- do
 - $\tau_{old} = \tau$;
 - let τ_1 be the weighted average of gray levels less than τ with weights $H(i)$, $i = 0, 1, \dots, \tau - 1$;
 - let τ_2 be the weighted average of gray levels greater than τ with weights $H(i)$, $i = \tau + 1, \tau + 2, \dots, 255$;
 - let $\tau = (\tau_1 + \tau_2)/2$;

until $|\tau - \tau_{old}| < T$.

In this way, every rectangle with a not empty intersection with the ROI has a different threshold. Let R_j , $j = 0, 1, \dots, J$ be the intersection of such rectangles and the ROI, and let τ_j ,

$j = 0, 1, \dots, J$ be the corresponding thresholds. The following Algorithm 2 computes the segmentation of the ROI in terms of n_F , i.e., the number of pixels in the fat mass, and n_L , i.e., the number of pixels in the lean mass.

Algorithm 2: (image segmentation). Let d be the diagonal of the rectangles in the partition of the ROI, and c_j be the center of the j -th rectangle. Given the sub-images $R_j, j = 0, 1, \dots, J$, and the corresponding thresholds $\tau_j, j = 0, 1, \dots, J$; compute n_F and n_L as the total number of pixels in the fat mass and in the lean mass, respectively, by the following steps

- $n_F = 0$;
 - $n_L = 0$;
 - for every pixel p in the ROI,
 - let R_j be the sub-image containing p , and $d_j = |c_j - p|$;
 - let $R_l, l = 1, 2, \dots, L$ be all the sub-images such that $|c_l - p| < |c_j - c_l|$ and $|c_l - p| < d$;
 - let $d_l = |c_l - p|, l = 1, 2, \dots, L$ and

$$\tau = \frac{d_j \tau_j + \sum_{l=1}^L d_l \tau_l}{d_j + \sum_{l=1}^L d_l} \quad (2)$$
 - if $GL(p) > \tau$, increase n_F by 1, else increase n_L by 1.
-

We note that in Algorithm 2, $GL(p)$ denotes the gray level of pixel p ; moreover, index L may be zero, for example, when sub-image R_j is near the boundary of the ROI; in this case, the summations appearing in the definition of τ must be considered equal to zero and $\tau = \tau_j$.

Therefore, the computation of parameter ρ is performed by Algorithm 1, Algorithm 2, and, finally, Formula (1).

2.2.3. Computation of Index β (Lacunarity)

Lacunarity analysis was performed by adopting the method previously developed in our laboratory as described in [33,34] and modified in [35,36].

Our method to estimate lacunarity is based on the gliding box algorithm (GBA). This algorithm computes the lacunarity of a set by analyzing its mass distribution [43]. More precisely, for a box (i.e., square) of side length $b > 0$, all the possible positions on the set (i.e., the ROI) and the mass of the set within each box are considered. In this way, a frequency distribution of the box mass is obtained and the lacunarity index β is computed by considering the moments of this distribution for different values of $b > 0$.

In this particular case, the set is the ROI under analysis (LeanCSA) and the set mass is the pixel gray level. So, an image segmentation is not strictly required for lacunarity analysis; however, a preprocessing step with a sigmoid function can improve the quality of the results. In particular, for each pixel p in the ROI, this step computes the new gray level $GP'(p)$ of p from the original value $GP(p)$ by using the following formula:

$$GP'(p) = \frac{1}{1 + \exp(-k(GP(p) - \sigma))}, \quad p \text{ in the ROI}, \quad (3)$$

where $k, \sigma > 0$ are two given parameters. It is worth noting that the procedure goes toward a complete binarization by increasing parameter k , related to sigmoid regularization.

For the sake of simplicity we assume that, for each b , only a finite number of masses $M_j, j = 1, 2, \dots, \eta(b)$ are encountered in the various gliding boxes of size b ; therefore, a discrete frequency distribution $n(M_j, b), j = 1, 2, \dots, \eta(b)$ has to be considered. Note that such an assumption holds for binary images, where the mass of a generic box on the image is given by the number of white pixels in the box, i.e., the pixels associated with the value one. From standard arguments on probability, the moments of order q of M are given by the following formula:

$$Z_q(M, b) = \frac{1}{N(b)} \sum_{j=1}^{\eta(b)} M_j^q n(M_j, b), \quad b > 0, \quad (4)$$

where the division by $N(b)$, i.e., the total number of boxes, needs to convert $n(M_j, b)$, $j = 1, 2, \dots, \eta(b)$ into a probability distribution. The definition of lacunarity function Λ uses only the first and the second moments of M , as follows:

$$\Lambda(b) = \frac{Z_2(M, b)}{Z_1(M, b)^2}, \quad b > 0. \quad (5)$$

We note that from the standard argument on probability theory, $\Lambda(b) > 1$, $b > 0$.

The GBA was implemented in software using MATLAB software package v. 7 (the MatWorks, Inc., Natick, MA, USA). The program begins to elaborate the ROI. Then, for each integer value of b between b_{min} and b_{max} , where b_{min} , b_{max} are given integer multiples of the pixel size in the image under consideration, the program computes the lacunarity function $\Lambda(b)$, $b = b_{min}, b_{min} + 1, \dots, b_{max}$ and shows the results on a graph.

As expected, for all images analyzed, the behavior of lacunarity function was a curvilinear plot resembling the hyperbola curve; therefore, the following model:

$$L(b) = \frac{\beta}{b^\alpha} + \gamma, \quad b \in [b_{min}, b_{max}] \quad (6)$$

was chosen to approximate the lacunarity function $\Lambda(b)$, where α, β, γ are suitable parameters.

This observation is consistent with the theoretical behavior of lacunarity function Λ for self-similar fractals and for other different random sets. Moreover, for such fractals, parameter α is related to the fractal dimension of the set and parameter β characterizes the lacunarity of the set, while γ represents the translation term on x axis [33,34].

In each particular example considered in this study, the best fit of lacunarity $\Lambda(b)$, $b = b_{min}, b_{min} + 1, \dots, b_{max}$, by the model function $L(b)$, $b \in [b_{min}, b_{max}]$, was computed as the solution of a least squares problem, where parameters α, β, γ are the independent variables. In particular, the minimizer of this problem is a triplet of parameters $(\alpha^*, \beta^*, \gamma^*)$ of the model function that better represents the variation in mass density of pixels in that image. Parameter β^* gives the lacunarity of the considered ROI.

Figure 2 (right) shows a schematic representation of our lacunarity analysis method.

2.2.4. Computation of Index μ (Succolarity)

Succolarity [42] refers to the capacity to allow for the flow of a fluid. So, it gives a further information with respect to fractal dimension and lacunarity since it depends on the spatial organization of lacunae, for example, into filaments through the set. We note that this fractal property is particularly relevant for the present analysis due to the geometrical organization of fatty infiltration into muscle tissue. Succolarity analysis was performed by refining the method presented in [41]. The proposed refinement is mainly based on the management of the different box sizes used to compute the flow of an ideal fluid through the ROI. Four main directions are considered, i.e., down to up, \uparrow ; left to right, \rightarrow ; up to down, \downarrow ; and right to left, \leftarrow ; however, here, we describe only the computation in the up to down case since the other ones can be obtained by proper rotations of the image. The capacity of a pixel p in the image to contain the fluid is given by $GL(p)$, i.e., the gray level of pixel p . The succolarity algorithm starts by flowing the pixels p of the ROI perimeter above the diagonals of the bounding box of the ROI. We note that the flowing operation is just given by a labeling operation and it needs to compute the pressure; in fact, pressure $\pi(p) = 0$ is assigned to these pixels. For each b between b_{min} and b_{max} , the following iterative procedure is performed: let π be the pressure of the pixels flooded in the previous step; from these pixels, the fluid flows to the pixels at (chessboard) distance less than or equal to b ; the pressure of these new flooded pixels is $\pi + 1$. When all the pixels are flooded, the succolarity function S_\downarrow is computed as follows:

$$S_\downarrow(b) = \frac{\sum_{p \in ROI} GL(p) \pi(p)}{\sum_{p \in ROI} \pi(p)}. \quad (7)$$

Proper rotations of the ROI can be used to compute the other succolarity functions S_{\leftarrow} , S_{\uparrow} , S_{\rightarrow} by the same procedure. From functions S_d , $d \in \{\downarrow, \leftarrow, \uparrow, \rightarrow\}$, the succolarity indices μ_{\downarrow} , μ_{\leftarrow} , μ_{\uparrow} , μ_{\rightarrow} are computed as follows:

$$\mu_d = \max\{S_d(b), \quad b \in [b_{\min}, b_{\max}]\}, \quad d \in \{\downarrow, \leftarrow, \uparrow, \rightarrow\}. \quad (8)$$

3. Results

3.1. Mass Composition of Paraspinal Muscles

The results on paraspinal muscle composition confirm an age-related decreasing trend for lean mass and an increasing trend for fatty mass. These results are consistent with those reported in the literature for different muscles [19–24]. The Lean/Fat ratio results of TotCSA show an age-related decreasing trend. In osteoporosis, the Lean/Fat ratio lower than that of the age-matched control group reflects the higher fatty mass in disease than in aging as both show similar amounts of lean mass. Table 2 summarizes classic measurement results on paraspinal muscle composition (area in pixel, percentage, and ratio) expressed as mean \pm SD of the average of the right and left paraspinal muscle groups.

Table 2. Paraspinal muscle composition by classic estimates.

Subjects	TotCSA	LeanCSA *	FatCSA †	Lean/Fat Ratio
All	11,114 \pm 1858	8507 \pm 2608 (77%) *	1925 \pm 1153 (23%)	4.40 \pm 3.53
Young	11,222 \pm 1939	9364 \pm 1929 (84%)	1858 \pm 1015 (16%)	7.17 \pm 5.73
Pre-menopause	10,652 \pm 1686	8481 \pm 1105 (80%)	2171 \pm 838 (20%)	4.34 \pm 1.35
Menopause	11,062 \pm 2043	8332 \pm 1609 (75%)	2730 \pm 1226 (25%)	3.50 \pm 1.54
Age-matched ¹	10,356 \pm 1215	7714 \pm 1364 (75%)	2642 \pm 1018 (25%)	3.51 \pm 1.87
Osteoporosis ²	11,517 \pm 1865	7837 \pm 1449 (68%)	3680 \pm 1315 (32%)	2.52 \pm 1.34

Values are mean \pm standard deviation expressed in pixel; * percentage values within round brackets are % of LeanCSA referred to TotCSA; † percentage values within round brackets are % of FatCSA referred to TotCSA; CSA: cross-sectional area; ¹ age-matched control group for comparison with Osteoporosis group; ² osteoporosis: bone mineral density T-score ≤ -2.5 as defined by the World Health Organization.

Figure 3 shows that osteoporotic subjects, when compared with age-matched controls, have an opposite trend of Lean/Fat ratio that is in contradiction with muscle composition, expressed as mean \pm SD (Table 2). In fact, despite similar lean mass values, osteoporotic subjects show a higher amount of fatty mass when compared with age-matched controls (Figure 4). This would have to account for a more marked decreasing trend of Lean/Fat ratio.

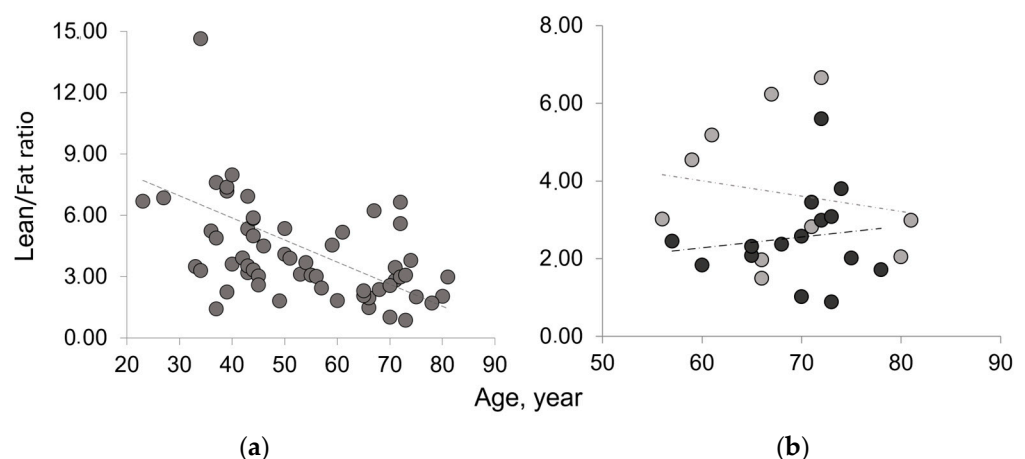


Figure 3. Lean/Fat ratio of the whole muscle mass area in aging and disease. (a) Age-related decreasing trend of Lean/Fat ratio in the whole sample analyzed; (b) comparison of Lean/Fat ratio between osteoporotic patients (black) and age-matched control group (gray) showing an increasing trend (dashed line) for osteoporotic group vs. a decreasing trend (dotted line) for age-matched controls.

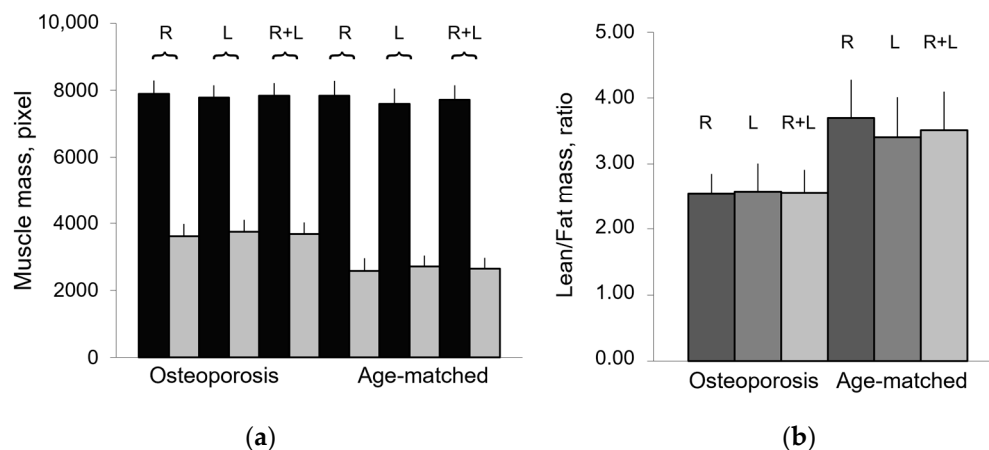


Figure 4. Composition of paraspinal muscles in aging and osteoporosis. (a) Lean mass (black) and fatty mass (gray) of paraspinal muscles, represented as mean values \pm SEM (standard error of mean) of right (R), left (L), and both (R + L) muscle groups, show comparable values between R and L groups; (b) Lean/Fat ratio of paraspinal muscles represented as mean value of right (R), left (L), and whole (R + L) muscle area.

3.2. Fractal Features of Paraspinal Muscle

To overcome this discrepancy, another index, lacunarity parameter β , was introduced to analyze the fatty infiltration of lean mass. Lacunarity analysis, in fact, provides a holistic estimate of muscle composition comprehensive of changes occurring at both lean and fatty muscle mass. In addition, to better characterize the fatty infiltration of the muscle, succolarity was also considered.

As comparable results of muscle composition were obtained for both right and left paraspinal muscles (Figure 4), additional analyses were performed only on the right paraspinal muscle group. In particular, parameter ρ (Lean/Fat ratio) and fractal features, parameter β (Lacunarity) and parameters μ (Succolarity) were used to quantify the fatty infiltration of lean muscle area, which are also potentially usable as indices of muscle contractile function.

Table 3 summarizes the results related to the three new indices proposed to quantify fatty infiltration. The results from the fractal analysis of right paraspinal muscles show that lacunarity parameter β , related to fatty infiltration, increases with age and physio-pathological status. In particular, osteoporosis and age-matched control groups are statistically significantly different ($p = 0.012$), with β values higher in osteoporosis than in 'healthy' aging. These results are consistent with fatty mass levels found higher in osteoporosis than in age-matched controls in spite of comparable lean mass levels. Figure 5 shows the age-related distribution of fatty infiltration expressed as lacunarity (parameter β) in the whole sample and in osteoporosis compared to the age-matched control group.

Lacunarity parameter α from our hyperbola model function-based lacunarity texture analysis, by correlating with fractal dimension, provides an estimate of the complexity of the lean muscle structure. Lacunarity parameter α values (Table 3) are higher in the young group and statistically significantly differ from the others ($p = 0.007, 0.017, 0.032$ respectively vs. pre-menopause, menopause, and osteoporosis groups). Osteoporosis and age-matched groups show similar values of parameter α ($p = 0.420$); nevertheless, they can be separated by lacunarity parameter β ($p = 0.012$).

Table 3. Fatty infiltration of paraspinal lean muscle mass.

Subjects	Young	Pre-Menopause	Menopause	Age-Matched	Osteoporosis	<i>p</i> Value ¹
Lean mass ²	8586 ± 1778	7889 ± 1002	7277 ± 1638	6581 ± 1024	6890 ± 1402	0.286
Fatty mass ²	2234 ± 756	2444 ± 732	2894 ± 936	2813 ± 1041	3627 ± 1114	0.046
Lean/Fat ratio ρ	4.21 ± 1.33	3.57 ± 0.68	2.70 ± 0.76	2.61 ± 0.89	2.08 ± 0.67	0.057
Lacunarity α	0.900 ± 0.403	0.572 ± 0.350	0.639 ± 0.303	0.672 ± 0.316	0.639 ± 0.420	0.420
Lacunarity β	0.062 ± 0.039	0.113 ± 0.040	0.101 ± 0.044	0.092 ± 0.041	0.148 ± 0.062	0.012
Succolarity μ_{\uparrow}	0.203 ± 0.075	0.243 ± 0.047	0.252 ± 0.070	0.253 ± 0.084	0.264 ± 0.077	0.371
Succolarity μ_{\rightarrow}	0.240 ± 0.085	0.288 ± 0.050	0.308 ± 0.070	0.298 ± 0.077	0.298 ± 0.080	0.499
Succolarity μ_{\downarrow}	0.243 ± 0.096	0.275 ± 0.042	0.276 ± 0.072	0.270 ± 0.086	0.283 ± 0.086	0.361
Succolarity μ_{\leftarrow}	0.218 ± 0.080	0.258 ± 0.042	0.267 ± 0.071	0.266 ± 0.084	0.263 ± 0.079	0.470

Results are mean ± standard deviation; ¹ *p* values calculated by one-tail *t*-test for $p \leq 0.05$ to compare differences between osteoporosis and age-matched control groups; ² lean and fatty mass related to lean muscle area (LeanCSA); α and β : fractal parameters from our hyperbola model method where α correlates with fractal dimension and β measures lacunarity, γ : the third coefficient from our hyperbola model method representing the translation term on *x* axis assumed a mean value ± standard deviation in the whole sample equal to 0.9818 ± 0.0370 ; μ_{\downarrow} , μ_{\leftarrow} , μ_{\uparrow} , μ_{\rightarrow} are the succolarity indices for the directions considered.

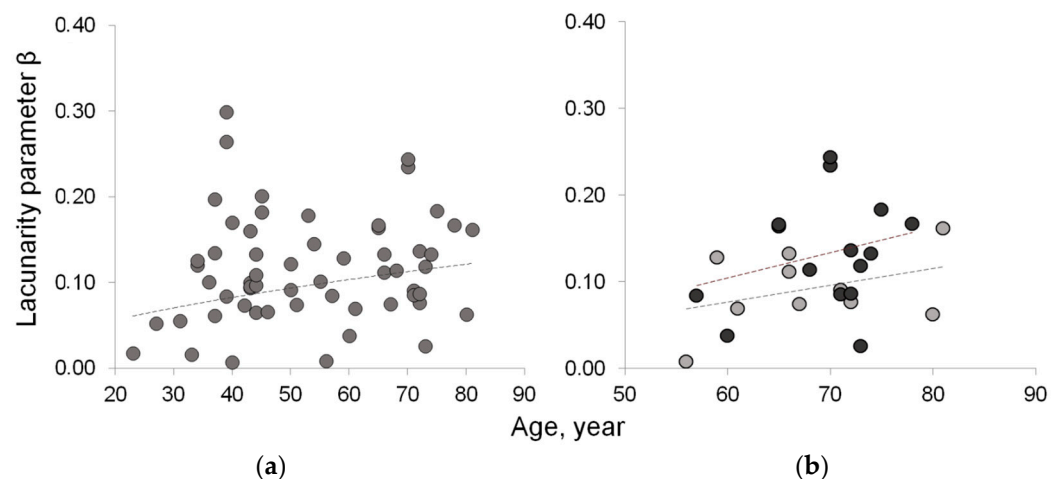


Figure 5. Lacunarity of lean muscle area to estimate muscle fatty infiltration. (a) Age-related increasing trend of lacunarity parameter β in the whole sample; (b) age-related distribution of lacunarity parameter β in osteoporotic patient (black circle) vs. age-matched controls (gray circle) shows similar increasing trend but with values higher in osteoporotic patients than in age-matched controls.

Figure 6 compares the fractal features used to measure lean muscle fatty infiltration (lacunarity parameter β and succolarity parameter μ for the four directions considered) in the groups of different age and physio-pathological status. Lacunarity can discriminate between osteoporosis and age-matched control groups ($p = 0.012$), while succolarity does not statistically change between aging and disease. It is worth noting that the groups showing similar lacunarity values (young, pre-menopause, and menopause) can be further discriminated by succolarity that shows increasing values of parameters μ from young to pre-menopause to menopause. In particular, the young group statistically significantly differs from both pre-menopause and menopause groups when the succolarity μ_{\uparrow} , μ_{\rightarrow} , and μ_{\leftarrow} values are considered (respectively, *p* values equal to 0.045, 0.035, and 0.049 in young vs. pre-menopause; *p* values equal to 0.043, 0.014, and 0.049 in young vs. menopause groups).

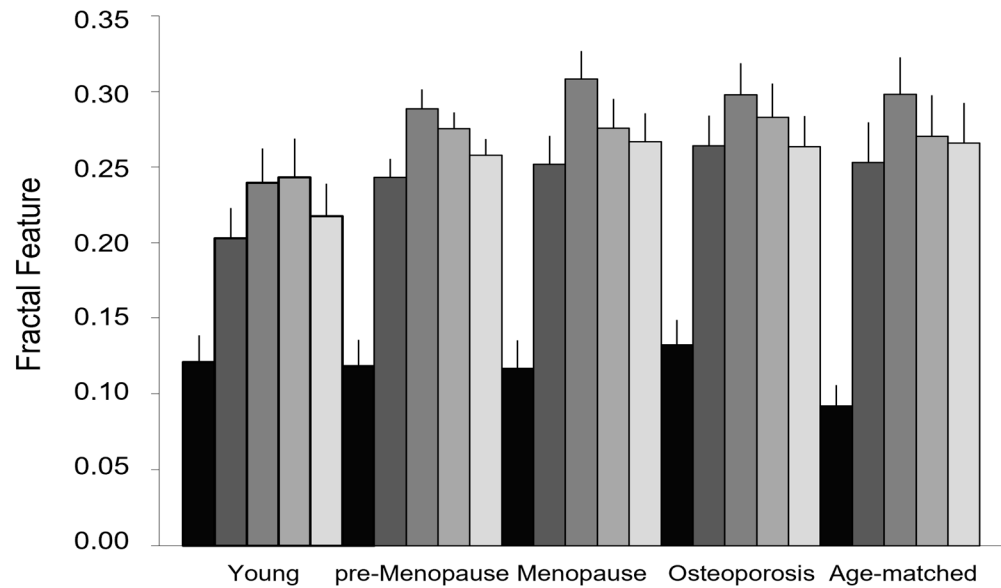


Figure 6. Fractal features of lean muscle area. Lacunarity and succolarity as indices of muscle fatty infiltration: lacunarity (black) discriminates between osteoporotic patients and age-matched controls but not among the other age and physio-pathological groups; succolarity (gray scale from dark to light gray for the four directions, \uparrow , \rightarrow , \downarrow , \leftarrow , respectively) shows increasing values from young to pre-menopause to menopause, the three age/physio-pathological groups showing similar lacunarity values. Data are represented as mean \pm SEM.

4. Discussion

In this study, we present a new method to quantify muscle fatty infiltration, an important index of muscle wasting usable in the diagnosis of sarcopenia. The method was set up taking into consideration the complexity of human beings and the pseudo-fractality of many biomedical structures and functions. It is worth noting that the mathematics of fractals, introduced to describe fractals in nature, has been developed on ideal fractals, characterized by self-similarity, and invariance of scale and fractal dimension was introduced to characterize a fractal. When we deal with natural objects, we have to face the problem of statistical similarity in a limited range of scale. Lacunarity and succolarity were introduced to better characterize fractal objects with the same fractal dimension but with a very different appearance. Lacunarity and succolarity analyses were then introduced for a better featuring of fractals. These fractal analyses were later introduced with a more general application as they represent texture analyses usable to describe complex patterns with fractal, multifractal, or no fractal properties, thus overcoming the limits of the fractal dimension applied to natural objects.

Given this premise and less strictly mathematically speaking, we show that fractal analysis can characterize muscle wasting better than classic methods. In particular, we found that lacunarity, as a tool to estimate the fatty infiltration of paraspinal muscles, is able to distinguish between aging and age-dependent disease (osteoporosis). In fact, fatty infiltration, as estimated by lacunarity parameter β , from our hyperbola-based method [34,36], increases with aging and it is statistically higher in osteoporotic patients than in healthy individuals with similar age.

It is worth noting that, in spite of the age-related increasing trend of lacunarity parameter β , lacunarity analysis fails to separate the other age/physio-pathological groups: young, pre-menopause, and menopause. However, succolarity analysis is able to discriminate among these three groups showing a similar lacunarity; parameter μ , used to quantify succolarity of paraspinal muscle in the four directions, is statistically significantly different among the three groups considered. These results are consistent with the use of succolarity to better characterize fractals showing the same lacunarity [39].

The need to consider new approaches to characterize muscle wasting with aging and pathology also stems from the lack of consistency of results on muscle composition based on classic measurements [44,45]. Our results on paraspinal muscle composition by classic measurements confirm an age-related decreasing trend for lean mass and an increasing trend for fatty mass. These results are consistent with those reported in the literature for different muscles [19–23,46]. The high degree of inter-individual variability observed, however, suggests introducing an alternative index able to correlate changes, positive and/or negative, occurring at the levels of both lean and fatty muscle mass. In fact, both inter- and intra-lean muscle infiltration of fatty tissue contribute to the reduction in contractile muscle responsible for altered muscle strength. Mechanical consequences on muscle function due to fat infiltration are not completely clear yet; however, it has been hypothesized that fat physically limits the strength of the muscle by interfering with its natural design [47]. It is known that mechanical stimulation induced by adequate training can favor muscle function preservation by reducing the accumulation of fat and adipose cells in the skeletal muscle [48].

In this study, we propose parameter ρ , an index representative of the ratio between lean and fatty mass in the whole muscle area (TotCSA) and in the muscle contractile area (LeanCSA), with the latter being used to obtain an index to provide an estimate of fatty infiltration of contractile muscle from classic measurements and, therefore, being better comparable with the new proposed fractal measurements. The Lean/Fat ratio results from TotCSA show that parameter ρ is lower in the osteoporosis group than in the age-matched control one. This is consistent with a higher fatty mass in osteoporotic patients than in the healthy aging control group in spite of similar lean muscle mass in the two groups. The results on parameter ρ from LeanCSA, as an estimate of fatty infiltration of contractile muscle, confirm higher amounts of fatty tissue in LeanCSA of osteoporotic patients than that of age-matched controls, showing similar amounts of lean tissue. This aspect accounts for the lower Lean/Fat ratio of LeanCSA in the osteoporosis group than in the age-matched control one. These results suggest that muscle contractile function could be more compromised in osteoporosis than in 'healthy' aging. However, in spite of such a difference between these two groups, parameter ρ is not able to separate osteoporotic patients from age-matched controls in a statistically significant manner. These observations need to be deepened in a larger sample where tests for muscle strength and function are also considered. Once more, we confirm that classic methods for muscle composition assessment lack a clear-cut conclusion by stressing the need for alternative and more effective approaches to characterize skeletal muscle wasting in sarcopenia.

Several factors are already known to play a role in the physiopathology of sarcopenia; nevertheless, its etiology has not been defined yet. From the literature, it emerges that different mechanisms combine to affect skeletal muscle physiology and contribute to the onset and progression of sarcopenia. Loss of regenerative capacity, denervation of muscle fibers, and increased inter- and intra-muscular infiltration of fat together with endocrine changes, mitochondrial dysfunction, oxidative stress, and inflammation are among the mechanisms that participate in the etiopathogenesis of sarcopenia [49,50]. Interestingly, as per other tissues or organs, most mechanisms involved in muscle wasting are strictly related to the aging processes.

Aging is characterized by functional and structural impairments at different levels and represents a critical risk factor for several chronic diseases. Different rates of aging processes that drive the biological aging of individuals are responsible for the high variability within and among individuals of a population even in the presence of homogeneous endogen and hexogen environments. Good biomarkers of aging [51,52] are, therefore, necessary to recognize physiological aging and separate normal from pathological aging, two main targets of aging studies dealing with aging in good health. It is worth nothing that gold-standard tools are not available yet to monitor physiological aging, nor have single measurements been qualified yet as good biomarkers of aging, sensitive and specific enough to distinguish normal aging from pathological aging [53].

To enlighten the search of good biomarkers of aging, contradictions and/or phenomena that appear incomprehensible can be clarified by paradigms such as complexity, chaos, and fractality. As a matter of fact, the marked inter- and intra-individual heterogeneity that characterizes the senescent phenotype can be justified by assuming the concept that longevity is a 'secondary product of evolution' of a nonlinear dynamic system [54,55].

Considering that complex systems are strictly dependent on their initial state, living beings in a cohort can be associated with complex systems [56] and any small perturbation occurring at certain times can be responsible for larger differences in most individual characteristics of the senescent phenotype later in the life. Therefore, from a practical point of view, the life trajectories of individuals in a population, although they may be close at birth, will progress with time following fluctuations that progressively increase the variance in their phenotype characteristics, such as aging (for more details, see [55,57]). The interindividual variability always present in an aging population is independent of environmental changes and can be observed even in the case of genetically homogeneous backgrounds. Genetic–environmental interactions induce unforeseeable behavior at critical points where life trajectories can change. Bifurcations, therefore, can be considered the origin of variability responsible for the heterogeneity that characterizes the senescent phenotype.

According to this setting, aging is the result of the time evolution of a complex system whose behavior is governed by the laws of chaos. Aging systems evolve with time by losing complexity [58]; this evolution is influenced by both endogenous and exogenous environmental factors. Humans, as complex systems governed by the laws of chaos, can generate so-called 'strange attractors' [59]. They are observable at bifurcations and can be described by fractals. Indeed, fractal analysis can represent a usable tool to describe biocomplexity and measure changes related to aging and pathology [60,61]. The senescent phenotype, influenced by specific individual genetic–environmental interactions, follows different trajectories with different kinetics rates, thus evolving as pathological aging (fast rate), physiological aging (intermediate rate), or successful aging (low rate) [36,57,62].

In this study, we demonstrate once more that fractal-derived methods represent powerful tools in the search of good biomarkers of aging since they can differentiate between physiological and pathological aging. They could also have potential to distinguish age-dependent from age-associated diseases, another major task to address aging in good health.

To the best of our knowledge, this is one among the rare studies aiming to quantify muscle fatty infiltration [63], and the first study approaching fractal featuring of muscle tissue. In fact, only muscle contractile function was previously described by fractal analysis of myographic waveforms [64]. Our results are from the middle axial section of the fourth lumbar vertebra based on our previous studies on vertebral trabecular bone performed in this section [34,36,65,66]. The goodness of our choice is also supported by the literature in the field, from which it emerges that, generally, fatty infiltration of paraspinal muscle increases from cranial to caudal, and the highest values have been detected at L4 and L5 [63,67,68]. Therefore, in the case of small variations in fatty infiltration, they could be detected in this site better than in other spine sites where fatty tissue is less represented.

Further studies are in progress on muscle fractal features in osteosarcopenia and bone fragility fracture risk. In this context, we have available data on muscle function and, therefore, by comparing fatty infiltration with muscle contractile function, we could be able to introduce our indices of lacunarity β and succolarity μ as usable in clinical settings to monitor both muscle composition and function. Improvements in the succolarity analysis method are also under consideration.

5. Conclusions

In this study, we demonstrate that fractal-derived methods can provide effective approaches to characterize muscle better than classic methods. In fact, lacunarity, by quantifying muscle fatty infiltration, is able to characterize age-related muscle wasting (sarcopenia) and to discriminate between normal aging and pathological aging (osteoporosis).

sis). Succolarity, the other measure introduced to characterize fractal objects with the same lacunarity, is able to discriminate among the three groups of age and physiological status (young, pre-menopause, and menopause), showing similar lacunarity values.

The original and innovative method proposed to quantify muscle fatty infiltration in MR images by fractal-derived indices such as lacunarity and succolarity can find applications in clinical settings as a sensitive tool to diagnose sarcopenia and monitor changes in muscle fatty infiltration as an index of muscle contractile function.

Finally, with this study, we further stress the relevance of introducing paradigms such as complexity, chaos, and fractality in the field of gerontology as they represent sources to obtain effective tools in the search of good biomarkers of aging and diseases.

Author Contributions: Conceptualization, A.Z.; methodology, A.Z. and P.M.; software, P.M. and M.Z.; validation, A.Z. and L.L.; formal analysis, A.Z. and P.M.; investigation, A.Z.; data curation, A.Z.; writing—original draft preparation, A.Z.; writing—review and editing, A.Z. and P.M. All authors have read and agreed to the published version of the manuscript.

Funding: This research received no external funding. This study was partially supported by the internal non-competing fund ‘Ricerca Corrente’ from the Italian Ministry of Health to IRCCS INRCA. The funder had no role in the study design, data collection, data analysis, data interpretation, or in writing the manuscript.

Institutional Review Board Statement: The dataset used in this study was from a database set up in 2005 for a previous study carried out in accordance with the Declaration of Helsinki and made available from our institute IRCCS INRCA after de-identification for scientific research reuse (GDPR EU 2016/679 and EU 2018/1807).

Informed Consent Statement: Patient consent was waived because we used a dataset made available for this study from our institute IRCCS INRCA after de-identification for scientific research reuse (GDPR EU 2016/679 and EU 2018/1807).

Data Availability Statement: The data presented in this study are available on request from the corresponding author.

Conflicts of Interest: The authors declare no conflicts of interest.

References

1. Evans, W.J. Skeletal muscle loss: Cachexia, sarcopenia, and inactivity. *Am. J. Clin. Nutr.* **2010**, *91*, 1123S–1127S. [[CrossRef](#)] [[PubMed](#)]
2. Evans, W.J.; Paolisso, G.; Abbatecola, A.M.; Corsonello, A.; Bustacchini, S.; Strollo, F.; Lattanzio, F. Frailty and muscle metabolism dysregulation in the elderly. *Biogerontology* **2010**, *11*, 527–536. [[CrossRef](#)] [[PubMed](#)]
3. Russ, D.W.; Grandy, J.S.; Toma, K.; Ward, C.W. Ageing, but not yet senescent, rats exhibit reduced muscle quality and sarcoplasmic reticulum function. *Acta Physiol.* **2011**, *201*, 391–403. [[CrossRef](#)] [[PubMed](#)]
4. Seene, T.; Kaasik, P.; Riso, E.M. Review on aging, unloading and reloading: Changes in skeletal muscle quantity and quality. *Arch. Gerontol. Geriatr.* **2012**, *54*, 374–380. [[CrossRef](#)] [[PubMed](#)]
5. Nielsen, B.R.; Abdulla, J.; Andersen, H.E.; Schwarz, P.; Suetta, C. Sarcopenia and osteoporosis in older people: A systematic review and meta-analysis. *Eur. Geriatr. Med.* **2018**, *9*, 419–434. [[CrossRef](#)] [[PubMed](#)]
6. Hida, T.; Shimokata, H.; Sakai, Y.; Ito, S.; Matsui, Y.; Takemura, M. Sarcopenia and sarcopenic leg as potential risk factors for acute osteoporotic vertebral fracture among older women. *Eur. Spine J.* **2016**, *25*, 3424–3431. [[CrossRef](#)]
7. Iida, H.; Sakai, Y.; Watanabe, T.; Matsui, H.; Takemura, M.; Matsui, Y. Sarcopenia affects conservative treatment of osteoporotic vertebral fracture. *Osteoporos Sarcopenia* **2018**, *4*, 114–117. [[CrossRef](#)] [[PubMed](#)]
8. Rosenberg, I.H. Summary comments: Epidemiological and methodological problems in determining nutritional status of older persons. *Am. J. Clin. Nutr.* **1989**, *50*, 1231–1233. [[CrossRef](#)]
9. Rosenberg, I.H. Sarcopenia: Origins and clinical relevance. *J. Nutr.* **1997**, *127*, 990S–991S. [[CrossRef](#)]
10. Delmonico, M.J.; Harris, T.B.; Lee, J.S.; Visser, M.; Nevitt, M.; Kritchevsky, S.B.; Tylavsky, F.A.; Newman, A.B.; Health, Aging and Body Composition Study. Alternative definitions of sarcopenia, lower extremity performance, and functional impairment with aging in older men and women. *J. Am. Geriatr. Soc.* **2007**, *55*, 769–774. [[CrossRef](#)]
11. Goodpaster, B.H.; Park, S.W.; Harris, T.B.; Kritchevsky, S.B.; Nevitt, M.; Schwartz, A.V.; Simonsick, E.M.; Tylavsky, F.A.; Visser, M.; Newman, A.B. The loss of skeletal muscle strength, mass, and quality in older adults: The health, aging and body composition study. *J. Gerontol. A Biol. Sci. Med. Sci.* **2006**, *61*, 1059–1064. [[CrossRef](#)] [[PubMed](#)]

12. Hiona, A.; Leeuwenburgh, C. The role of mitochondrial DNA mutations in aging and sarcopenia: Implications for the mitochondrial vicious cycle theory of aging. *Exp. Gerontol.* **2008**, *43*, 24–33. [[CrossRef](#)] [[PubMed](#)]
13. Marzetti, E.; Leeuwenburgh, C. Skeletal muscle apoptosis, sarcopenia and frailty at old age. *Exp. Gerontol.* **2006**, *41*, 1234–1238. [[CrossRef](#)] [[PubMed](#)]
14. Fearon, K.; Evans, W.J.; Anker, S.D. Myopenia—A new universal term for muscle wasting. *J. Cachexia Sarcopenia Muscle* **2011**, *2*, 1–3. [[CrossRef](#)] [[PubMed](#)]
15. Clark, B.C.; Manini, T.M. Functional consequences of sarcopenia and dynapenia in the elderly. *Curr. Opin. Clin. Nutr. Metab. Care* **2010**, *13*, 271–276. [[CrossRef](#)] [[PubMed](#)]
16. Gonzales, E.; Messi, M.L.; Delbono, O. The specific force of single intact extensor digitorum longus and soleus mouse muscle fibers declines with aging. *J. Membr. Biol.* **2000**, *178*, 175–183. [[CrossRef](#)] [[PubMed](#)]
17. Stackhouse, S.K.; Stevens, J.E.; Lee, S.C.; Pearce, K.M.; Snyder-Mackler, L.; Binder-Macleod, S.A. Maximum voluntary activation in nonfatigued and fatigued muscle of young and elderly individuals. *Phys. Ther.* **2001**, *81*, 1102–1109. [[CrossRef](#)]
18. Weisleder, N.; Brotto, M.; Komazaki, S.; Pan, Z.; Zhao, X.; Nosek, T.; Parness, J.; Takeshima, H.; Ma, J. Muscle aging is associated with compromised Ca²⁺ spark signaling and segregated intracellular Ca²⁺ release. *J. Cell. Biol.* **2006**, *174*, 639–645. [[CrossRef](#)] [[PubMed](#)]
19. Delmonico, M.J.; Harris, T.B.; Visser, M.; Park, S.W.; Conroy, M.B.; Velasquez-Mieyer, P.; Boudreau, R.; Manini, T.M.; Nevitt, M.; Newman, A.B.; et al. Longitudinal study of muscle strength, quality, and adipose tissue infiltration. *Am. J. Clin. Nutr.* **2009**, *90*, 1579–1585. [[CrossRef](#)]
20. Heymsfield, S.B.; Adamek, M.; Gonzalez, M.C.; Gia, G.; Thomas, D.M. Assessing skeletal muscle mass: Historical overview and state of the art. *J. Cachexia Sarcopenia Muscle* **2014**, *5*, 9–18. [[CrossRef](#)]
21. Cruz-Jentoft, A.J.; Baeyens, J.P.; Bauer, J.M.; Boirie, Y.; Cederholm, T.; Landi, F.; Martin, F.C.; Michel, J.P.; Rolland, Y.; Schneider, S.M.; et al. Sarcopenia: European consensus on definition and diagnosis: Report of the European Working Group on Sarcopenia in Older People. *Age Ageing* **2010**, *39*, 412–423. [[CrossRef](#)]
22. Cruz-Jentoft, A.J.; Bahat, G.; Bauer, J.; Boirie, Y.; Bruyère, O.; Cederholm, T.; Cooper, C.; Landi, F.; Rolland, Y.; Sayer, A.A.; et al. Sarcopenia: Revised European consensus on definition and diagnosis. *Age Ageing* **2019**, *48*, 16–31. [[CrossRef](#)] [[PubMed](#)]
23. Chianca, V.; Albano, D.; Messina, C.; Gitto, S.; Rufo, G.; Guarino, S.; Del Grande, F.; Sconfenza, L.M. Sarcopenia: Imaging assessment and clinical application. *Abdom. Radiol.* **2022**, *47*, 3205–3216. [[CrossRef](#)] [[PubMed](#)]
24. Heskamp, L.; Okkersen, K.; van Nimwegen, M.; Ploegmakers, M.J.; Bassez, G.; Deux, J.-F.; van Engelen, B.G.; Heerschap, A.; For the OPTIMISTIC Consortium. Quantitative Muscle MRI Depicts Increased Muscle Mass after a Behavioral Change in Myotonic Dystrophy Type 1. *Radiology* **2020**, *297*, 132–142. [[CrossRef](#)] [[PubMed](#)]
25. Goutallier, D.; Postel, J.M.; Bernageau, J.; Lavau, L.; Voisin, M.C. Fatty muscle degeneration in cuff ruptures. Pre- and postoperative evaluation by CT scan. *Clin. Orthop. Relat. Res.* **1994**, *304*, 78–83. [[CrossRef](#)]
26. Fortin, M.; Lazáry, Á.; Varga, P.P.; Battié, M.C. Association between paraspinal muscle morphology, clinical symptoms and functional status in patients with lumbar spinal stenosis. *Eur. Spine J.* **2017**, *26*, 2543–2551. [[CrossRef](#)] [[PubMed](#)]
27. Battaglia, P.J.; Maeda, Y.; Welk, A.; Hough, B.; Kettner, N. Reliability of the Goutallier classification in quantifying muscle fatty degeneration in the lumbar multifidus using magnetic resonance imaging. *J. Manip. Physiol. Ther.* **2014**, *37*, 190–197. [[CrossRef](#)] [[PubMed](#)]
28. Tamai, K.; Chen, J.; Stone, M.; Arakelyan, A.; Paholpak, P.; Nakamura, H.; Buser, Z.; Wang, J.C. The evaluation of lumbar paraspinal muscle quantity and quality using the Goutallier classification and lumbar indentation value. *Eur. Spine J.* **2018**, *27*, 1005–1012. [[CrossRef](#)] [[PubMed](#)]
29. Fortin, M.; Battie, M.C. Quantitative paraspinal muscle measurements: Intersoftware reliability and agreement using OsiriX and ImageJ. *Phys. Ther.* **2012**, *92*, 853–864. [[CrossRef](#)]
30. Armi, L.; Fekri-Ershad, S. Texture image analysis and texture classification methods—A review. *arXiv* **2019**. [[CrossRef](#)]
31. Zucker, S.W.; Terzopoulos, D. Finding structure in Co-occurrence matrices for texture analysis. *Comput. Graph. Image Process.* **1980**, *12*, 286–308. [[CrossRef](#)]
32. Addison, O.; Marcus, R.L.; LaStayo, P.C.; Ryan, A.S. Intermuscular Fat: A Review of the Consequences and Causes. *Int. J. Endocrinol.* **2014**, *2014*, 309570. [[CrossRef](#)] [[PubMed](#)]
33. Zaia, A.; Eleonori, R.; Maponi, P.; Rossi, R.; Murri, R. Medical imaging and osteoporosis: Fractal’s lacunarity analysis of trabecular bone in MR images. In Proceedings of the Eighteenth IEEE Symposium on Computer-Based Medical Systems (CBMS 2005), Dublin, Ireland, 23–24 June 2005; IEEE: New York, NY, USA, 2005; pp. 3–8. [[CrossRef](#)]
34. Zaia, A.; Eleonori, R.; Maponi, P.; Rossi, R.; Murri, R. MR imaging and osteoporosis: Fractal lacunarity analysis of trabecular bone. *IEEE Trans. Inf. Technol. Biomed.* **2006**, *10*, 484–489. [[CrossRef](#)] [[PubMed](#)]
35. Zaia, A.; Rossi, R.; Egidi, N.; Maponi, P. Fractal’s lacunarity analysis of trabecular bone in MR images. In *Computational Vision and Medical Image Processing*; Tavares, J., Jorge, N., Eds.; CRC Press: Boca Raton, FL, USA, 2010; pp. 421–426.
36. Zaia, A. Fractal lacunarity of trabecular bone and magnetic resonance imaging: New perspectives for osteoporotic fracture risk assessment. *World. J. Orthop.* **2015**, *6*, 221–235. [[CrossRef](#)] [[PubMed](#)]
37. Mandelbrot, B.B. A Fractal’s Lacunarity, and how it can be Tuned and Measured. In *Nonnenmacher TF, Losa GA, Weibel ER, editors. In Fractals in Biology and Medicine*; Birkhauser Press: Basel, Switzerland, 1993; pp. 8–21.

38. Plotnick, R.E.; Gardner, R.H.; Hargrove, W.W.; Prestegard, K.; Perlmutter, M. Lacunarity analysis: A general technique for the analysis of spatial patterns. *Phys. Rev. E* **1996**, *53*, 5461–5468. [[CrossRef](#)] [[PubMed](#)]
39. Mandelbrot, B.B. The Fractal Geometry of Nature. In *Trees and the Diameter Exponent*; WH Freeman: New York, NY, USA, 1977; pp. 156–165.
40. Metze, K.; Adam, R.; Florindo, J.B. The fractal dimension of chromatin—A potential molecular marker for carcinogenesis, tumor progression and prognosis. *Expert Rev. Mol. Diagn.* **2019**, *19*, 299–312. [[CrossRef](#)] [[PubMed](#)]
41. de Melo, R.H.C.; Conci, A. How Succolarity could be used as another fractal measure in image analysis. *Telecommun. Syst.* **2013**, *52*, 1643–1655. [[CrossRef](#)]
42. de Melo, R.H.C.; Conci, A. Succolarity: Defining a method to calculate this fractal measure. In Proceedings of the 15th International Conference on Systems, Signals and Image Processing, Bratislava, Slovakia, 25–28 June 2008; pp. 291–294. [[CrossRef](#)]
43. Allain, C.; Cloitre, M. Characterizing the lacunarity of random and deterministic fractal sets. *Phys. Rev. A* **1991**, *44*, 3552–3558. [[CrossRef](#)] [[PubMed](#)]
44. Shur, N.F.; Creedon, L.; Skirrow, S.; Atherton, P.J.; MacDonald, I.A.; Lund, J.; Greenhaff, P.L. Age-related changes in muscle architecture and metabolism in humans: The likely contribution of physical inactivity to age-related functional decline. *Ageing Res. Rev.* **2021**, *68*, 101344. [[CrossRef](#)]
45. Volpi, E.; Nazemi, R.; Fujita, S. Muscle tissue changes with aging. *Curr. Opin. Clin. Nutr. Metab. Care* **2004**, *7*, 405–410. [[CrossRef](#)]
46. Pang, J.; Tu, F.; Han, Y.; Zhang, E.; Zhang, Y.; Zhang, T. Age-related change in muscle strength, muscle mass, and fat mass between the dominant and non-dominant upper limbs. *Front. Public Health* **2023**, *11*, 1284959. [[CrossRef](#)] [[PubMed](#)]
47. Rahemi, H.; Nigam, N.; Wakeling, J.M. The effect of intramuscular fat on skeletal muscle mechanics: Implications for the elderly and obese. *J. R. Soc. Interface* **2015**, *12*, 20150365. [[CrossRef](#)]
48. Emanuelsson, E.B.; Berry, D.B.; Reitzner, S.M.; Arif, M.; Mardinoglu, A.; Gustafsson, T.; Ward, S.R.; Sundberg, C.J.; Chapman, M.A. MRI characterization of skeletal muscle size and fatty infiltration in long-term trained and untrained individuals. *Physiol. Rep.* **2022**, *10*, e15398. [[CrossRef](#)] [[PubMed](#)]
49. Budui, S.L.; Rossi, A.P.; Zamboni, M. The pathogenetic bases of sarcopenia. *Clin. Cases Miner. Bone Metab.* **2015**, *12*, 22–26. [[CrossRef](#)] [[PubMed](#)]
50. Scicchitano, B.M.; Pelosi, L.; Sica, G.; Musarò, A. The physiopathologic role of oxidative stress in skeletal muscle. *Mech. Ageing Dev.* **2017**, *170*, 37–44. [[CrossRef](#)] [[PubMed](#)]
51. Johnson, T.E. Recent results: Biomarkers of aging. *Exp. Gerontol.* **2006**, *41*, 1243–1246. [[CrossRef](#)] [[PubMed](#)]
52. Wagner, K.-H.; Cameron-Smith, D.; Wessner, B.; Franzke, B. Biomarkers of Aging: From Function to Molecular Biology. *Nutrients* **2016**, *8*, 338. [[CrossRef](#)] [[PubMed](#)]
53. Burkle, A.; Moreno-Villanueva, M.; Bernhard, J.; Blasco, M.; Zondag, G.; Hoeijmakers, J.H.; Toussaint, O.; Grubeck-Loebenstein, B.; Mocchegiani, E.; Collino, S.; et al. Mark-age biomarkers of ageing. *Mech. Ageing Dev.* **2015**, *151*, 2–12. [[CrossRef](#)] [[PubMed](#)]
54. Piantanelli, L.; Rossolini, G.; Basso, A.; Piantanelli, A.; Malavolta, M.; Zaia, A. Use of mathematical models of survivorship in the study of biomarkers of aging: The role of heterogeneity. *Mech. Ageing Dev.* **2001**, *122*, 1461–1475. [[CrossRef](#)]
55. Zaia, A. Osteoporosis and fracture risk: New perspectives for early diagnosis and treatment assessment. In *Osteoporosis: Etiology, Diagnosis and Treatment*; Mattingly, B.E., Pillare, A.C., Eds.; Nova Science Publishers: Hauppauge, NY, USA, 2009; pp. 267–290.
56. Pettersson, M. *Complexity and Evolution*; Cambridge University Press: Cambridge, UK, 1996.
57. Zaia, A.; Maponi, P. Mitochondrial DNA Profiling by Fractal Lacunarity to Characterize the Senescent Phenotype as Normal Aging or Pathological Aging. *Fractal Fract.* **2022**, *6*, 219. [[CrossRef](#)]
58. Lipsitz, L.A.; Goldberger, A.L. Loss of ‘complexity’ and aging: Potential applications of fractals and chaos theory to senescence. *JAMA* **1992**, *267*, 1806–1809. [[CrossRef](#)]
59. Grassberger, A.; Procaccia, I. Measuring the strangeness of strange attractors. *Phys. D Nonlinear Phenom.* **1983**, *9*, 189–208. [[CrossRef](#)]
60. Goldberger, A.L.; Rigney, D.R.; West, B.J. Chaos and fractals in human physiology. *Sci. Am.* **1990**, *262*, 42–49. [[CrossRef](#)] [[PubMed](#)]
61. Goldberger, A.L. Non-linear dynamics for clinicians: Chaos theory, fractals, and complexity at the bedside. *Lancet* **1996**, *347*, 1312–1314. [[CrossRef](#)] [[PubMed](#)]
62. Franceschi, C.; Garagnani, P.; Morsiani, C.; Conte, M.; Santoro, A.; Grignolio, A.; Monti, D.; Capri, M.; Salvioli, S. The Continuum of Aging and Age-Related Diseases: Common Mechanisms but Different Rates. *Front. Med.* **2018**, *5*, 61. [[CrossRef](#)] [[PubMed](#)]
63. Mandelli, F.; Nüesch, C.; Zhang, Y.; Halbeisen, F.; Schären, S.; Mündermann, A.; Netzer, C. Assessing Fatty Infiltration of Paraspinal Muscles in Patients with Lumbar Spinal Stenosis: Goutallier Classification and Quantitative MRI Measurements. *Front. Neurol.* **2021**, *12*, 656487. [[CrossRef](#)] [[PubMed](#)]
64. Coelho, A.L.V.; Lima, C.A.M. Assessing fractal dimension methods as feature extractors for EMG signal classification. *Eng. Appl. Artif. Intell.* **2014**, *36*, 81–98. [[CrossRef](#)]
65. Zaia, A.; Rossi, R.; Galeazzi, R.; Sallei, M.; Maponi, P.; Scendoni, P. Fractal lacunarity of trabecular bone in vertebral MRI to predict osteoporotic fracture risk in over-fifties women. The LOTO study. *BMC Musculoskelet. Disord.* **2021**, *22*, 108. [[CrossRef](#)] [[PubMed](#)]
66. Zaia, A.; Maponi, P.; Sallei, M.; Galeazzi, R.; Scendoni, P. Measuring Drug Therapy Effect on Osteoporotic Fracture Risk by Trabecular Bone Lacunarity: The LOTO Study. *Biomedicines* **2023**, *11*, 781. [[CrossRef](#)]

-
67. Kjaer, P.; Bendix, T.; Sorensen, J.S.; Korsholm, L.; Leboeuf-Yde, C. Are MRI-defined fat infiltrations in the multifidus muscles associated with low back pain? *BMC Med.* **2007**, *5*, 2. [[CrossRef](#)]
 68. Lee, J.C.; Cha, J.G.; Kim, Y.; Kim, Y.I.; Shin, B.J. Quantitative analysis of back muscle degeneration in the patients with the degenerative lumbar flat back using a digital image analysis: Comparison with the normal controls. *Spine* **2008**, *33*, 318–325. [[CrossRef](#)] [[PubMed](#)]

Disclaimer/Publisher’s Note: The statements, opinions and data contained in all publications are solely those of the individual author(s) and contributor(s) and not of MDPI and/or the editor(s). MDPI and/or the editor(s) disclaim responsibility for any injury to people or property resulting from any ideas, methods, instructions or products referred to in the content.